JOURNAL OF BACTERIOLOGY, Feb. 2008, p. 1419–1428 Vol. 190, No. 4
0021-9193/08/$08.00+0 doi:10.1128/JB.01414-07

Interaction of CheY with the C-Terminal Peptide of CheZ▽†

Jayita Guhaniyogi,[1,2] Ti Wu,[1,3] Smita S. Patel,[2] and Ann M. Stock[1,2,3]*

Center for Advanced Biotechnology and Medicine, 679 Hoes Lane, Piscataway, New Jersey 08854[1]; Department of Biochemistry, University of Medicine and Dentistry of New Jersey, Robert Wood Johnson Medical School, Piscataway, New Jersey 08854[2]; and Howard Hughes Medical Institute, 679 Hoes Lane, Piscataway, New Jersey 08854[3]

Received 31 August 2007/Accepted 4 December 2007

Chemotaxis, a means for motile bacteria to sense the environment and achieve directed swimming, is controlled by flagellar rotation. The primary output of the chemotaxis machinery is the phosphorylated form of the response regulator CheY (P∼CheY). The steady-state level of P∼CheY dictates the direction of rotation of the flagellar motor. The chemotaxis signal in the form of P∼CheY is terminated by the phosphatase CheZ. Efficient dephosphorylation of CheY by CheZ requires two distinct protein-protein interfaces: one involving the strongly conserved C-terminal helix of CheZ ($CheZ_C$) tethering the two proteins together and the other constituting an active site for catalytic dephosphorylation. In a previous work (J. Guhaniyogi, V. L. Robinson, and A. M. Stock, J. Mol. Biol. 359:624–645, 2006), we presented high-resolution crystal structures of CheY in complex with the $CheZ_C$ peptide that revealed alternate binding modes subject to the conformational state of CheY. In this study, we report biochemical and structural data that support the alternate-binding-mode hypothesis and identify key recognition elements in the CheY-$CheZ_C$ interaction. In addition, we present kinetic studies of the $CheZ_C$-associated effect on CheY phosphorylation with its physiologically relevant phosphodonor, the histidine kinase CheA. Our results indicate mechanistic differences in phosphotransfer from the kinase CheA versus that from small-molecule phosphodonors, explaining a modest twofold increase of CheY phosphorylation with the former, observed in this study, relative to a 10-fold increase previously documented with the latter.

The specific swimming behavior of a bacterial cell subject to its chemical environment is governed by the direction of flagellar rotation (2, 3, 48). The response regulator CheY is a central component of bacterial chemotaxis. Along with its cognate histidine kinase, CheA, CheY constitutes the well-conserved two-component phosphotransfer pathway transducing signals from the environment via the transmembrane chemoreceptors to the flagellar motor. This signal transduction cascade regulates a steady-state level of phosphorylated CheY (P∼CheY), which dictates the direction of flagellar rotation. Phosphorylation of CheY enhances its affinity for FliM, a component of the flagellar motor, inducing clockwise flagellar rotation and tumbly behavior.

Cellular concentrations of P∼CheY are regulated by a delicate balance of incoming phosphoryl groups from the kinase CheA and outgoing phosphoryl groups owing to both CheY autodephosphorylation and dephosphorylation mediated by its phosphatase, CheZ. Efficient dephosphorylation of CheY by CheZ requires the formation of an active site for dephosphorylation and tethering of the two proteins to each other (35, 52). The latter involves interaction of P∼CheY with the strongly conserved C-terminal region of CheZ ($CheZ_C$) (4). The binding of $CheZ_C$ to P∼CheY is essential for CheZ-mediated dephosphorylation (4, 35). The minimum region sufficient for binding to CheY spans the C-terminal 19 residues of CheZ ($CheZ_{C19}$), residues 196 to 214, bearing the sequence AGVV ASQDQVDDLLDSLGF (4).

In a previous article (13) describing high-resolution crystal structures of both inactive CheY and CheY activated with the phosphoryl analog BeF_3^- in complex with a synthetic $CheZ_C$ peptide ($CheZ_{C15}$), we showed that the $CheZ_{C15}$ peptide binds to both inactive and active CheY in alternate orientations (state-specific dual binding model) (see Fig. 1), and in the case of inactive CheY, it binds to a meta-active conformation, providing an explanation for the previously observed increase in binding affinity for the $CheZ_{C19}$ peptide with CheY phosphorylation (26) and the enhancement in the CheY phosphorylation rate with small-molecule phosphodonors (35). However, the extent of lattice bias on both the observed alternate binding mode and the meta-active conformation of CheY in the inactive CheY-$CheZ_{C15}$ structures was unclear. Here we present equilibrium binding studies with mutant $CheZ_C$ peptides, a 2.6-Å crystal structure of CheY-BeF_3^- bound to the $CheZ_{C19}$ peptide with an extended N terminus relative to the one previously used (13) and a 2.7-Å crystal structure of the inactive CheY-$CheZ_{C15}$ complex in a crystal lattice different from the one formerly described (13). All support the conformational state-specific dual-binding-mode hypothesis unbiased by lattice conformations. In addition, our binding studies reveal the significance of the strongly conserved C-terminal Phe214 residue of CheZ as an anchor in the molecular recognition mechanism between CheY and $CheZ_C$.

Furthermore, studies on $CheZ_C$-associated enhancement of CheY phosphorylation have thus far been limited to phosphotransfer from small-molecule phosphodonors (13, 35). Here we present kinetic studies of $CheZ_C$-associated acceleration of CheY phosphorylation from its physiologically relevant phos-

* Corresponding author. Mailing address: Center for Advanced Biotechnology and Medicine, 679 Hoes Lane, Piscataway, NJ 08854. Phone: (732) 235-4844. Fax: (732) 235-5289. E-mail: stock@cabm.rutgers.edu.

† Supplemental material for this article may be found at http://jb.asm.org/.

▽ Published ahead of print on 14 December 2007.

TABLE 1. Peptides and corresponding sequences

Peptide	Sequence[a]
WT $CheZ_{C15}$	Ac-ASQDQVDDLLDSLG F-OH
WT $CheZ_{C19}$	Ac-AGVVASQDQVDDLL DSLGF-OH
$WT_{nonac}CheZ_{C19}$	AGVVASQDQVDDLLDS LGF-OH
$CheZ_{C19amide}$	Ac-AGVVASQDQVDDLL DSLGF-NH_2
$CheZ_{C19}$ ^{214}Phe→Ala	Ac-AGVVASQDQVDDLL DSLGA-OH
$CheZ_{C19}$ ^{202}Gln→Ala^{206} Asp→Ala	Ac-AGVVASADQVADLL DSLGF-OH

[a] N-terminal acetyl groups are denoted by "Ac" and C-terminal carboxylate and amide groups by "OH" and "NH_2," respectively.

TABLE 2. Primers and sequences

Construct	Primer	Sequence
$CheA_{FL}$, $CheA_{\Delta P2}$	NdeI_forward	GGTGATCATATGAGCAT GGATATTAGC
$CheA_{FL}$, $CheA_{\Delta P2}$	SalI_reverse	CTTCTCGTCGACTCAGG CGGCTGTGATCGC
$CheA_{\Delta P2}$	BamHI_reverse	TGGGGATCCTGCTGCTG GTGCTGGCTGGATCG CCGCGCTTAG
$CheA_{\Delta P2}$	BamHI_forward	GCAGGATCCCCACCACG AGCGTCAGCGGAACA TCATGCGGGG
$CheA_{\Delta P2}$	Linker_forward	TCGACGGATCCTCTAGA
$CheA_{\Delta P2}$	Linker_reverse	AGCTTCTAGAGGATCCG

phodonor, phosphorylated CheA (P~CheA). Our results suggest mechanistic differences between two sources of phosphoryl groups for CheY—small molecules and P~CheA. Their significance in the context of bacterial chemosensory signaling is discussed.

MATERIALS AND METHODS

Peptides and oligonucleotides. $CheZ_C$ peptides and oligonucleotides are listed in Tables 1 and 2, respectively. Unless otherwise indicated to be nonacetylated with the subscript "nonac", all peptides used in this study were acetylated at the N termini. The $CheZ_C$ peptides used for crystallization were obtained from the peptide synthesis core facility of Massachusetts General Hospital (Boston, MA) and those for binding and quench flow experiments from the Louisiana State University Protein Facility (Baton Rouge, LA). The oligonucleotides used for CheA plasmid constructions were obtained from Integrated DNA Technologies (Coralville, IA).

Lyophilized peptides were initially dissolved in a minimal amount of 1 M triethyl ammonium acetate (TEAA) buffer (90358; Fluka), followed by dilution in water to a final concentration of 20 mM. The peptide solutions, subsequently stored as lyophilized aliquots at −80°C, were dissolved in respective buffers to yield 20 mM working stock solutions and subjected to centrifugation before each use. The peptide content for peptides used in the binding experiments was determined by amino acid analyses by the LSU protein facility (Baton Rouge, LA), and peptide stability was assessed by UV absorbance at 220 nm on a Nanodrop ND-1000 spectrophotometer before each use.

Chemicals. The ammonium salt of the small-molecule phosphodonor phosphoramidate was synthesized as previously described (36). [γ-^{32}P]ATP with a specific activity of 5,000 Ci per mmol was purchased from GE Healthcare. All other reagent-grade chemicals used in the experiments were obtained from standard commercial sources.

Proteins. A pUC12-based *Salmonella enterica* CheY expression vector, pME124 (27, 43), was used for CheY expression. The *S. enterica cheA* gene (accession code J03611) (41) from the T7 expression vector pJES307 (46) (pAS2) was subcloned using a double-stranded-DNA linker (Table 2) into the NdeI-HindIII site, replacing the *cheR* gene within the CheR expression plasmid, pME43 (38), to create the $CheA_{FL}$ expression plasmid pJG4. The *S. enterica* $CheA_{\Delta P2}$ construct was created by removing the P2 coding region (residues 150 to 263) and joining the flanking linker regions with a proline-rich linker having the sequence PAPAAGSPPRASA, similar but not identical to the previously described *Escherichia coli* $CheA_{\Delta P2}$ construct (40). The *cheA*$_{\Delta P2}$ coding region was first cloned into the T7 expression vector, pJES307 (46), to create the $CheA_{\Delta P2}$ expression vector pJG2 using the BamHI_forward and BamHI_reverse primers (Table 2) encoding the 13-residue flexible linker and then cloned into the NdeI-HindIII site of pME43 to create the $CheA_{\Delta P2}$ expression plasmid pJG3.

Protein expression and purification. Expression plasmids for CheY, $CheA_{FL}$, and $CheA_{\Delta P2}$ were transformed into HB101 cells. All proteins were purified with fast-performance liquid chromatography using an AKTA system (GE Healthcare), using columns from GE Healthcare. The CheY protein was purified by a modification of previously described procedures (42). The previously used ion exchange and gel filtration columns were replaced with a HiTrap Q Fast Flow 26/20 column and a Superdex 75 26/60 column, respectively. Both CheA proteins were purified by a series of DEAE-Sepharose 26/20, CHT-II 26/20, butyl Sepharose, and Superdex 200 26/60 columns. The purified proteins were quantitated by measuring UV absorbance at 280 nm using extinction coefficients (ε_{280}) of 0.493, 0.220, and 0.258 ml mg^{-1} cm^{-1} for CheY, $CheA_{FL}$, and $CheA_{\Delta P2}$, respectively, calculated from the amino acid composition (12).

Crystallization. The crystallization protocol using the hanging drop method was followed as previously described (13). Crystallization of the CheY-BeF_3^--$CheZ_{C19}$ complex was achieved with 1.0 mM CheY and 1.5 mM $CheZ_{C19}$ in 50 mM HEPES (pH 7.0) (buffer A) with 10 mM $MgCl_2$, 5 mM $BeCl_2$, and 30 mM NaF and with reservoir solutions containing 0.1 M ammonium thiocyanate and 37.5% PEG-8000 in 0.1 M 2-(*N*-morpholino)-ethanesulfonic acid (MES) (pH 6.0). The CheY-$CheZ_{C15}$ crystals in this study were generated using CheY and the $CheZ_{C15}$ peptide in buffer A at 1:1.5 molar ratios with CheY concentrations ranging between 0.1 and 1.0 M and the peptide concentrations between 0.15 and 1.5 M, respectively, under identical precipitant conditions. Cryoprotection was achieved as previously described (13). NaF and $BeCl_2$ were included in the cryosolution in the case of the BeF_3^--bound crystal.

Data collection and processing. In the case of CheY-BeF_3^--$CheZ_{C19}$, 200° of data with 1° width were collected to 2.6 Å at beamline X4C, and in the case of CheY-$CheZ_{C15}$, 360° of data with 1° width were collected to 2.7 Å, at beamline X4A at the National Synchrotron Light Source at Brookhaven National Laboratory, Upton, NY. Reflections were indexed and integrated using the DENZO software program (29), and the processed images were scaled using the SCALEPACK software program (29). Data collection and processing statistics are listed in Table 3. Space groups were determined using a combination of SCALEPACK statistics, output from the Matthews probability calculator server (http://www.ruppweb.org/mattprob/) (14, 24), and inspection of systematic absences along the screw axes using the HKLVIEW program (8). For the CheY-BeF_3^--$CheZ_{C19}$ and CheY-$CheZ_{C15}$ structures, the data processed in the $P2_12_12$ and $P1$ space groups with three and four molecules per asymmetric unit with a Matthews coefficient of 2.4 $Å^3$/Da and 2.1 $Å^3$/Da, yielding a solvent content of 49% and 41.5%, respectively.

Structure determination and refinement. Both the CheY-BeF_3^--$CheZ_{C19}$ and CheY-$CheZ_{C15}$ structures were solved using the molecular replacement program Phaser (33, 44), using as a search molecule a polyalanine model of the CheY-BeF_3^- crystal structure (PDB identifier [ID] 1FQW) lacking the β4-α4 loop (residues 88 to 92) (19). Subsequent steps in structure refinement were performed using the CCP4 4.2.2 program suite (8). The intensities obtained from SCALEPACK were converted to structure factor amplitudes using the software program TRUNCATE (11), followed by a rigid-body refinement, density modification with solvent flipping, histogram matching, and noncrystallographic symmetry averaging using the software program Refmac 5.1.24 (28). Subsequently, iterative cycles of maximum likelihood and isotropic temperature factor refinement and model building using the software program O were performed until convergence. Water molecules were initially modeled using the ARP-wARP routine (18), and subsequently only waters and other small molecules with Fourier difference peaks greater than 3σ were included in the final models. The translation/libration/screw motion determination protocol using the TLSMD server (http://skuld.bmsc.washington.edu/~tlsmd/) (30, 31) was used to determine the optimal number of translation/libration/screw groups and generate parameters that were used in the final stages of refinement in the software program Refmac 5.1.2.4 (28). Initial models for MES were obtained from the Hic-up server (http://xray.bmc.uu.se/hicup/) (17). Refinement statistics are listed in

TABLE 3. Data collection and refinement statistics

Parameter	Value for data or structure[a]	
	CheY-CheZ$_{C15}$	CheY-CheZ$_{C19}$
Data collection		
Wavelength	0.97931	0.9795
Lattice	P_1	$P2_12_12$
Cell		
a, b, c (Å)	34.8, 53.7, 65.6	65.1, 163.0, 37.3
α, β, γ (°)	90.2, 102.9, 90.2	90.0, 90.0, 90.0
Resolution (Å)	30.0–2.7 (2.8–2.7)	30.0–2.6 (2.7–2.6)
R_{sym}[b]	0.061 (0.508)	0.137 (0.350)
Completeness (%)	98.8 (98.4)	99.5 (99.2)
Redundancy	3.9 (3.9)	8.4 (8.6)
$I/\sigma I$	22.4 (2.8)	15.4 (6.4)
Refinement		
Resolution (Å)	30.0–2.7	30.0–2.6
R_{work}[c]	0.205	0.213
R_{free}[d]	0.285	0.274
No. of reflections	11,332	12,004
No. of protein atoms	2039	3308
No. of small molecules		
Magnesium ion	2	3
BeF_3^-	0	3
MES	0	1
Water	16	54
rmsd values from ideality		
Bond lengths (Å)	0.012	0.014
Bond angles (°)	1.033	1.124
Avg B value for all atoms (Å^2)	33.6	22.2

[a] Values corresponding to highest-resolution shells are shown in parentheses.
[b] R_{sym}, $(\Sigma|I_{obs} - I_{avg}|)/(\Sigma I_{avg})$, where I_{obs} is the observed integrated intensity and I_{avg} is the average integrated intensity from multiple measurements.
[c] R_{work}, $(\Sigma||F_{obs}|_{(hkl)} - |F_{calc}|_{(hkl)}|)/(\Sigma|F_{obs}|_{(hkl)})$, where F_{obs} and F_{calc} are the observed and calculated structure factor amplitudes for *hkl* indices, respectively.
[d] R_{free} is identical to R_{work} but is calculated from 10% of the reflections set aside as a disjoint set prior to refinement.

Table 3. In the case of CheY-CheZ$_{C19}$, the three CheY molecules in each asymmetric unit have low main-chain root mean square deviation (rmsd) values ranging between 0.32 Å and 0.39 Å, whereas the three CheZ$_{C19}$ molecules differ in the degree of disorder in the solvent-exposed terminal regions, limiting the inclusion of terminal residues in the final model. In the case of CheY-CheZ$_{C15}$, two CheY chains have bound Mg^{2+} and two have bound water molecules at the active sites in spite of the absence of $MgCl_2$ from the crystallization solutions. The two CheY chains with bound Mg^{2+} differ from the latter by having main-chain rmsd values ranging between 0.55 Å and 0.57 Å.

Structural analyses. Least-square superpositions of atomic models and estimates of differences in tertiary structure by δ_3-rmsd analyses were performed as previously described (13, 15). Peptide-CheY contact analyses were performed using the software programs CNS 1.1 (6) and iMOLTALK version 2.0 (10) and the protein-protein interaction server (http://www.biochem.ucl.ac.uk/bsm/PP/server/). The lattice contact analyses were performed using the WHATIF web interface (http://swift.cmbi.kun.nl/WIWWWI/) (47). All structural figures were generated using the Pymol software program (9).

Equilibrium binding analyses. Dissociation constants (K_d values) for CheY-CheZ$_C$ binding were measured by equilibrium binding analyses, following the change in CheY intrinsic fluorescence in the conserved Trp58 adjacent to the active site Asp57 (23). Fluorescence measurements were performed with a CheY sample in a 2-ml reaction buffer containing 0.1 M HEPES and 10 mM $MgCl_2$ (pH 7.0) (buffer B) in a 10- by 10- by 40-mm quartz cuvette with continuous stirring on a Fluoromax-2 spectrofluorometer (Jobin Yvon; Spex Instruments S.A., Inc.) with an excitation wavelength at 280 nm. For each set, 5-μl aliquots of a peptide stock in buffer B were added to the CheY sample using the PB-600 repeating dispenser attached to a 250-μl Hamilton syringe (Hamilton Company) and stirred for 1 min before fluorescence measurement. Optimal fits subject to individual binding affinities were obtained using different concentrations of CheY and the peptide stock, different emission wavelengths (340 to 410 nm), and different excitation and emission slit widths (0.6 to 2.0 nm), ensuring a linear range for all measured intensities. Each set was repeated three times, and the average values for the dissociation constants and the respective standard errors are reported (Table 4). Fluorescence measurements with P~CheY were performed as previously described using phosphoramidate as the phosphodonor (23, 26). The effect of increased ionic strength due to phosphoramidate on peptide binding was examined with the CheZ$_{C19amide}$ peptide in the presence and absence of 0.1 M phosphoramidate in a buffer containing 0.1 M HEPES (pH 7.0)–0.1 mM EDTA, without Mg^{2+}, a condition under which CheY phosphorylation does not occur. The K_d values obtained after fitting the data, as described below, were within 1 standard deviation (~7%), although the absolute fluorescence change is significantly greater in the presence of 0.1 M phosphoramidate (data not shown).

TABLE 4. Binding analyses

Peptide	K_d (μM)[a]	
	Inactive CheY	P~CheY
WT$_{nonac}$CheZ$_{C19}$	206.9 ± 15.4	15.1 ± 0.1
WT CheZ$_{C19}$	67.4 ± 4.5	2.2 ± 0.2
CheZ$_{C19}$ ^{202}Q→A,^{206}D→A	110.0 ± 9.2	19.5 ± 0.6
CheZ$_{C19amide}$	156.3 ± 12.5	7.9 ± 0.1
CheZ$_{C19}$ ^{214}F→A	471.9 ± 26.0	53.2 ± 0.9
WT CheZ$_{C15}$	64.7 ± 3.1	13.2 ± 2.1

[a] Standard errors from triplicate experiments are listed.

The data were treated as in a previous bimolecular binding study (20). The fluorescence values were corrected for sample dilution according to equation 1,

$$F_{corr} = F_{obs}\frac{V_0 + V_p}{V_0} \quad (1)$$

where F_{corr} is the corrected fluorescence, F_{obs} is the observed fluorescence, V_0 is the initial sample volume, and V_p is the cumulative volume of the peptide added. The fluorescence intensities from the peptide samples by themselves were not significant. The corrected fluorescence intensities were plotted against the total peptide concentration and were fitted to equations 2 and 3,

$$F_{corr} = f_Y([Y_t] - [YZ_C]) + f_{YZ_C}[YZ_C] \quad (2)$$

where f_Y is the fluorescence coefficient of free CheY, f_{YZc} is the fluorescence coefficient of CheY bound to the CheZ$_C$ peptide, $[Y_t]$ is the total CheY protein concentration, and $[YZ_C]$ is the concentration of CheY bound to the CheZ$_C$ peptide, which can be further defined as

$$[YZ_C] = \frac{K_d + [Y_t] + [Z_C] - \sqrt{(K_d + [Y_t] + [Z_C])^2 - 4[Y_t][Z_C]}}{2} \quad (3)$$

where K_d is the dissociation constant and $[Z_C]$ is the total CheZ$_C$ peptide concentration. The data were analyzed using the Sigmaplot 8.0 software program (Systat Software, Inc.) with f_Y, f_{YZc}, and K_d treated as fittable parameters.

Phosphorylation of CheA proteins. The purified CheA$_{FL}$ and CheA$_{ΔP2}$ proteins, at final concentrations of 5 μM, were phosphorylated with 1 mM [γ-^{32}P]ATP with a specific activity of ~2,000 cpm/pmol of phosphoryl groups at 20°C for 20 min in a buffer containing 50 mM Tris (pH 7.5), 50 mM KCl, 5 mM $MgCl_2$, and 0.5 mM dithiothreitol (buffer C) with 0.5 mM EDTA. Phosphorylated proteins were then purified as the void volume eluent on EconoPak 10DG prepacked disposable columns (Bio-Rad), preequilibrated with buffer C. The concentration of phosphorylated protein was determined by filter binding assays using nitrocellulose paper squares following four consecutive washes under highly alkaline conditions with 50 mM Na_2CO_3 to maintain the acid-labile phosphohistidine bonds. From the specific activity and protein concentration, it is estimated that under these conditions, ~90% of CheA is phosphorylated. Purified proteins were stored at −20°C for up to a week prior to use.

CheY phosphorylation kinetics. All CheY phosphotransfer experiments with radiolabeled P~CheA proteins were performed using a KinTek Corporation RQF-3 rapid quench instrument with a buffer containing 50 mM Tris, 50 mM KCl, and 10 mM $MgCl_2$ (pH 7.5) (buffer D), with temperatures maintained at 8°C for experiments with P~CheA$_{FL}$ and at 25°C for experiments with P~CheA$_{ΔP2}$ using a circulating water bath, by rapidly mixing 30.5 μl of 0.1 μM

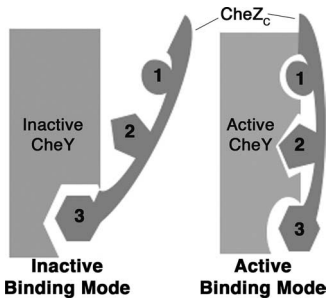

FIG. 1. Schematic illustration of the state-specific dual-binding model. Discrete modes of $CheZ_C$ peptide binding to CheY are correlated with different conformational states of CheY, i.e., inactive binding mode for binding to inactive CheY and active binding mode for binding to activated CheY. The $CheZ_C$ peptide binds to the α4-β5-α5 surface of CheY in both modes. In the inactive mode, the majority of the interactions are through C-terminal Phe214 (residue no. 3; depicted as hexagons) and the N terminus is exposed to the solvent; in the active mode, the surface buried by C-terminal Phe214 is reduced while electrostatic contacts involving N-terminal residues Gln202 (residue no. 1; depicted as circles) and Asp206 (residue no. 2; depicted as pentagons) are responsible for burying the N terminus of the $CheZ_C$ peptide to the α4-β5-α5 face of CheY. In the absence of CheY activation, when the $CheZ_C$ peptide is bound in the inactive mode, CheY is in a meta-active state (13).

$P\sim CheA_{FL}$ or $P\sim CheA_{\Delta P2}$ with 27.5 μl of CheY at concentrations ranging between 2 μM and 40 μM in the presence or absence of 2 mM $CheZ_{C15}$ peptide. At predetermined time points ranging from 5 to 200 ms, achieved by using a variable reaction loop volume, each reaction was terminated with ~96.9 μl of 0.1 M EDTA in 50 mM Tris (pH 7.5) (quench buffer) and expelled into a collection tube containing 51.5 μl of 10% sodium dodecyl sulfate in bromophenol blue solution (loading buffer) with no further second delay time.

A 12-μl aliquot of each sample was loaded onto a 26-well 18% Tris-HCl Criterion gel (Bio-Rad) and run in duplicate for 45 min in a Criterion cell (Bio-Rad) at 170 V at 4°C. Complete time courses were analyzed on the same gel. Gels were immediately blotted with Kimwipes, wrapped in plastic wrap, exposed to a PhosphorImager screen (Molecular Dynamics) for 12 h, and scanned using a PhosphorImager scanner (Molecular Dynamics). The band intensity (arbitrary units) was determined using ImageQuant software. Each reaction was performed in two independent experiments, and within each experiment, duplicate aliquots were analyzed on separate gels. The levels of P~CheA in the samples relative to those at the zero time points were averaged and used for the analysis.

Observed rate constants (k_{obs}) were generated by fitting the time courses to single exponentials by using the Sigmaplot 8.0 program (Systat Software, Inc.). The k_{obs} values were then plotted against the final CheY concentrations and were treated according to the kinetic model as previously described (25). Under the experimental conditions, phosphotransfer from P~CheA to CheY follows pseudo-first-order kinetics (25), displaying saturation kinetics with $P\sim CheA_{FL}$, described by a rectangular hyperbola, treating the first-order phosphorylation rate and the dissociation constant for the $P\sim CheA_{FL} \cdot$ CheY complex as fittable parameters (39), and no saturation with $P\sim CheA_{\Delta P2}$, described by a straight line, treating the second-order phosphorylation rate as a fittable parameter (40) in k_{obs}-versus-[CheY] plots.

Protein data bank accession numbers. The coordinates and structure factors for BeF_3^--bound CheY-$CheZ_{C19}$ and for BeF_3^--free CheY-$CheZ_{C15}$ have been deposited in the RCSB Protein Data Bank with the PDB IDs 2PL9 and 2PMC, respectively.

RESULTS

Equilibrium binding analyses of CheY-$CheZ_C$. Previously reported structures of inactive and activated CheY bound to the $CheZ_{C15}$ peptide (13) clearly demonstrate the correlation between alternate binding modes and CheY conformation that forms the basis of the state-specific binding model, schematically depicted in Fig. 1. To test this binding model, equilibrium binding analyses were performed with inactive CheY and CheY phosphorylated with phosphoramidate (see Materials and Methods) using peptides with mutations disrupting each binding mode-specific contact (Fig. 1) revealed by the previous structural analyses (13). Representative binding curves for the wild-type (WT) $CheZ_{C15}$ peptide for binding inactive CheY and P~CheY are shown in Fig. 2, and average K_d values for all peptides analyzed are reported in Table 4.

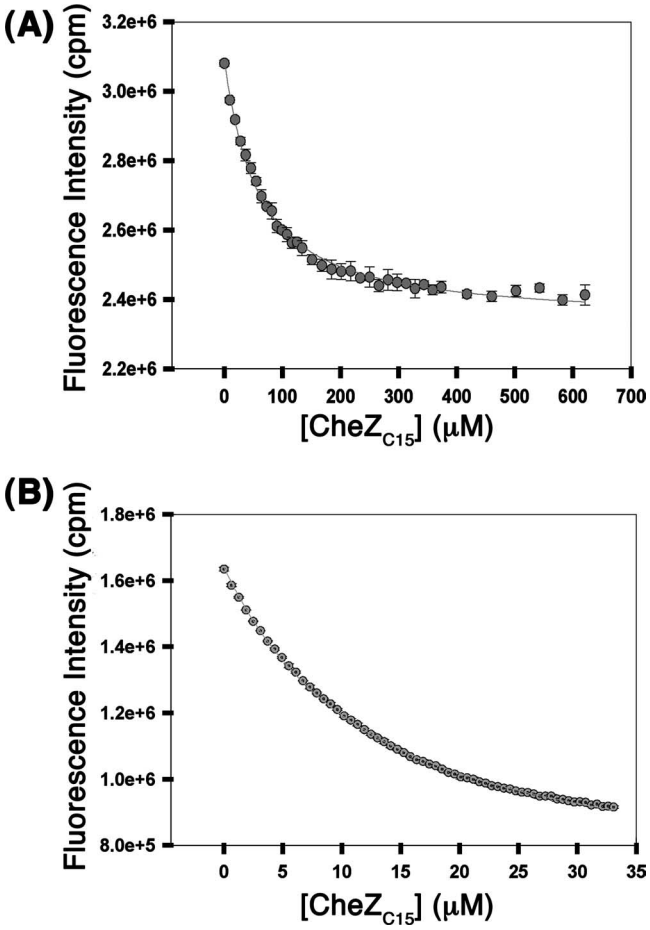

FIG. 2. Binding of the WT $CheZ_{C19}$ peptide to inactive CheY (A) or CheY activated with 0.1 M phosphoramidate (B). Peptide binding was assayed by measurement of intrinsic fluorescence of CheY Trp58 using excitation and emission wavelengths of 280 nm and 346 nm, respectively. The average scaled fluorescence intensities with standard errors of replicates are shown. The data for inactive CheY were generated with 10 μM CheY using slit widths of 0.6 nm and for P~CheY, with 2 μM CheY using slit widths of 2 nm.

Peptides used in the biochemical and structural analyses were typically acetylated at their N termini to more closely replicate the noncharged backbone of the extended polypeptide chain. However, we examined one nonacetylated peptide ($WT_{nonac}CheZ_{C19}$) to allow comparison with data from a previous study (26). Dissociation constants (K_d) for the *S. enterica* WT $CheZ_{C19}$ peptide without N-terminal acetylation (WT_{nonac} $CheZ_{C19}$) are similar (within twofold) to those previously reported for the *E. coli* system (26). Acetylation of the N terminus of the WT peptide (WT $CheZ_{C19}$) increases binding affin-

ities (decreases K_d) for inactive CheY by 2.3-fold and those to P~CheY by 6.8-fold.

The mutant peptide CheZ$_{C19}$ Gln202Ala Asp206Ala, in which the active binding mode-specific contacts involving residues Gln202 and Asp206 are disrupted, displayed a marginally weaker binding affinity (1.6-fold higher K_d) for inactive CheY but a significantly weaker affinity (8.9-fold higher K_d) for P~CheY relative to results for the WT CheZ$_{C19}$ peptide. The CheZ$_{C19amide}$ mutant peptide, in which the inactive binding mode-specific contact involving the C-terminal carboxyl group is disrupted, showed almost equally weak affinities for both inactive CheY and P~CheY. The effect of the mutation of the C-terminal Phe214 residue to Ala (i.e., CheZ$_{C19}$ Phe214Ala) was the most drastic, with 7-fold-weaker binding to inactive CheY and 24-fold-weaker binding to P~CheY. Additionally, binding analyses were performed with the WT CheZ$_{C15}$ peptide, identical to the one used in the previously reported CheY-CheZ$_{C15}$ structural studies, in which four residues at the N terminus are truncated relative to the WT CheZ$_{C19}$ peptide. N-terminal truncation had no effect on binding to inactive CheY but weakened binding to activated CheY (sixfold higher K_d) relative to results for the WT CheZ$_{C19}$ peptide.

Structural analysis of BeF_3^--bound CheY-CheZ$_{C19}$. Equilibrium binding analyses indicated that P~CheY binds to CheZ$_{C19}$ with higher binding affinity than that for CheZ$_{C15}$ while inactive CheY binds to both peptides with similar affinities (Table 4). To explain the difference in binding affinities between the CheZ$_{C19}$ and CheZ$_{C15}$ peptides and activated CheY, crystal structures were pursued. While biochemical studies typically employ phosphoramidate as the small-molecule phosphodonor to phosphorylate CheY, the phospho-Asp thus generated is too labile for crystallographic analysis. Hence, BeF_3^- was used as a noncovalent phosphoryl analog to mimic the activated CheY protein in the structural studies (51). A crystal of *S. enterica* WT BeF_3^-- activated CheY in complex with a synthetic CheZ$_{C19}$ peptide was generated as detailed in Materials and Methods, diffracted to 2.6 Å, and found to belong to the $P2_12_12$ space group. The structure was solved and refined as described in Materials and Methods. Data collection and refinement statistics are presented in Table 3.

In the CheY-BeF_3^--CheZ$_{C19}$ structure, CheY is fully activated, similar to CheY-BeF_3^- (PDB ID 1FQW) (19), since a comparison of the CheY molecules in the two structures yields the following: (i) low average values of rmsd upon superposition of main-chain atoms of CheY (0.39 Å) and (ii) identical active-site geometry, similar positions of switch regions (Thr87, β4-α4 loop, and Tyr106), and a smaller magnitude of tertiary structure difference in the switch regions, as quantified by δ_3-rmsd (data not shown).

Superposition of the main-chain atoms of the CheY molecules in the previously reported CheY-BeF_3^--CheZ$_{C15}$ (PDB ID 2FMK) (13) and CheY-BeF_3^--CheZ$_{C19}$ structures shows high similarity except for a small deviation in the angle of the peptide helices (Fig. 3A). Contact analysis shows that the CheZ$_{C19}$ peptides in the two complexes exhibit the same set of H-bond and Van der Waals contacts (Fig. 3B). The position of the CheZ$_{C19}$ peptide does not appear to be influenced by any noncrystallographic or specific symmetry contacts. Lattice interactions involving the peptide include only three nonspecific van der Waals contacts at distances more than 3.7 Å with symmetry-related CheY molecules (data not shown). In addition to the common set of contacts characterizing the active binding mode, the CheZ$_{C19}$ peptide participates in three additional specific contacts (an H bond between the backbone carbonyl of CheY Ala90 and the backbone amide of CheZ$_C$ Val199 and between CheY Lys92 and backbone groups of CheZ$_C$ Ala196 and Gly197 and hydrophobic contacts involving Val199), as well as several nonspecific van der Waals contacts between the N-terminal extended region of the CheZ$_{C19}$ peptide and the CheY β4-α4 loop. These additional contacts offered by the extended N terminus in CheZ$_{C19}$ relative to CheZ$_{C15}$ account for the increased binding affinities for activated CheY and the CheZ$_{C19}$ and CheZ$_{C15}$ peptides (Table 4). These contacts are likely to exist in the full-length protein. Thus, the CheZ$_{C19}$ peptide is a more physiologically relevant model than the CheZ$_{C15}$ peptide.

Structural analysis of inactive CheY-CheZ$_{C15}$ in the *P*1 lattice. In the previously characterized complexes of inactive CheY-CheZ$_{C15}$, crystallized in the *F*432 space group, the peptide molecules are involved in symmetry contacts through nonspecific van der Waals interactions, raising a question of the influence of lattice contacts on the observed peptide orientation (13). Crystallization and characterization of the inactive CheY-CheZ$_{C15}$ peptide complex in a space group different from *F*432 was undertaken to rule out this lattice bias. A crystal of *S. enterica* CheY bound to the CheZ$_{C15}$ peptide, diffracting to 2.7 Å with data processing in the triclinic *P*1 space group, was used for structure determination (Materials and Methods). Data collection and refinement statistics are presented in Table 3.

The CheZ$_{C15}$ peptide in the structure displays a complicated binding mode shared between two symmetry-related CheY molecules, imposed by lattice restrictions (see Fig. S1 in the supplemental material). Apparently as a consequence of this shared binding, electron density in this region was diffuse and peptide atoms refined with high B-factors, although all side chains for CheZ$_{C15}$ residues 206 to 214 were included in the final model. Of these, side chains for Phe214 and Asp210 were well ordered; density for the side chains of Leu208 and Leu212 was weak, and that for the remaining residues was nonexistent. However, based on the angle of the helical axis, it is clear that the CheZ$_{C15}$ peptide in the structure is bound in the inactive binding mode (Fig. 3C). Furthermore, conformational analyses indicated that the conformation of CheY in the structure approximates a "meta-active" state, similar to the one observed in the previously reported CheY-CheZ$_{C15}$ structures solved in the *F*432 lattice (13) (Fig. 3D; also data not shown). The highly similar peptide orientation and CheY conformation in structures of the inactive complex solved from crystals belonging to two different space groups with different lattice interactions provide structural evidence against lattice bias in the mode of interaction of the peptide with inactive CheY.

Kinetic analysis of CheY phosphorylation in the presence and absence of the CheZ$_{C15}$ peptide with P~CheA. Peptide-associated acceleration of the rate of phosphoryl transfer to CheY from small-molecule phosphodonors has been established (35). To address the effect of the CheZ$_C$ peptide on CheY phosphotransfer from its physiologically relevant phosphodonor, kinase CheA, the rates of phosphotransfer from

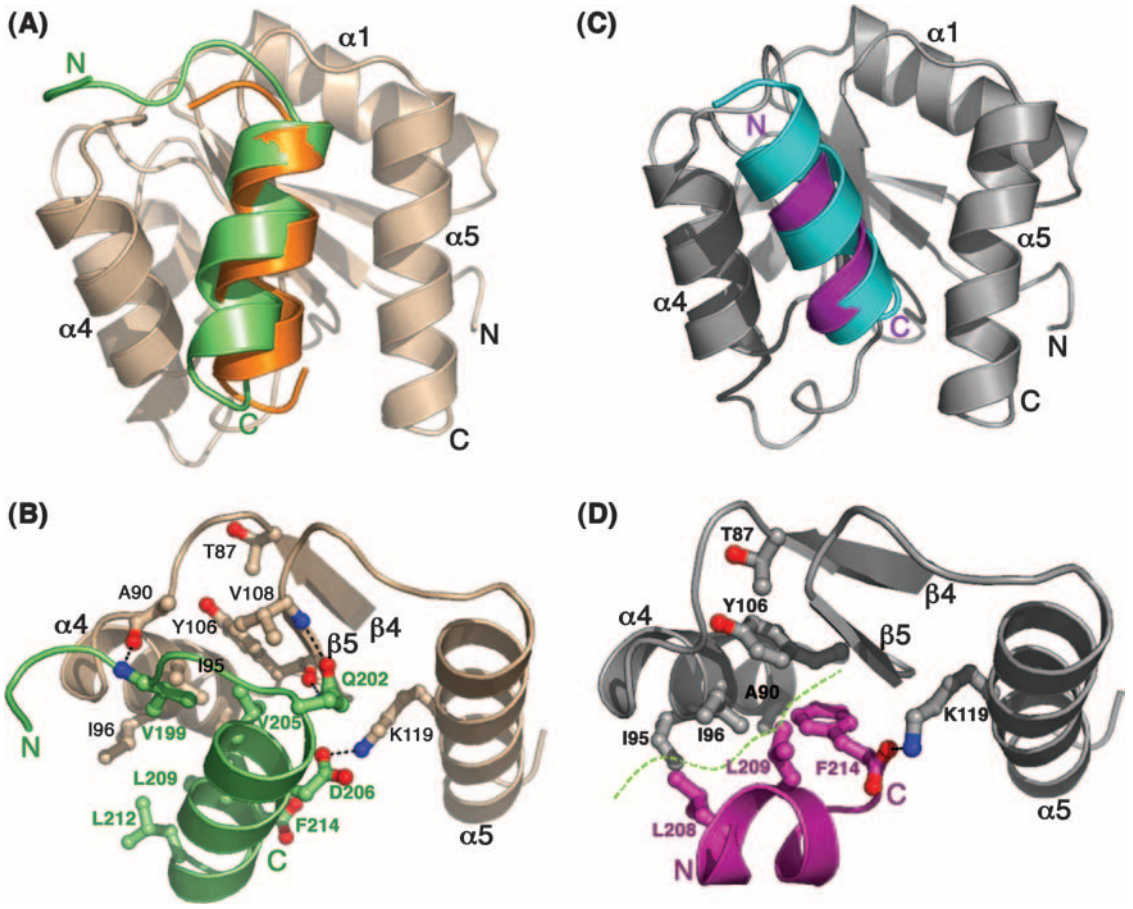

FIG. 3. Mode of $CheZ_C$ binding in CheY-$CheZ_C$ complexes. (A) Orientations of the $CheZ_C$ helices in BeF_3^--bound CheY-$CheZ_{C19}$ (PDB ID 2PL9) and BeF_3^--bound CheY-$CheZ_{C15}$ (PDB ID 2FMK) structures upon superposition of CheY main-chain atoms. The CheY molecule is shown in wheat and the $CheZ_C$ peptides in green and orange. (B) Specific interactions between the α4-β5-α5 region of CheY (wheat) and the $CheZ_{C19}$ peptide (green) in BeF_3^--bound CheY-$CheZ_{C19}$. (C) Orientations of the $CheZ_C$ helices in the BeF_3^--free CheY-$CheZ_{C15}$ structure solved from a *P*1 crystal (PDB ID 2PMC) and the BeF_3^--free CheY-$CheZ_{C15}$ structure solved from an *F*432 crystal (PDB ID 2FMH) upon superposition of CheY main-chain atoms. The CheY molecule is shown in gray and the $CheZ_C$ peptides in purple and cyan. (D) Specific interactions between the α4-β5-α5 region of CheY (gray) and the $CheZ_{C15}$ peptide (purple) in BeF_3^--free CheY-$CheZ_{C15}$ solved from a *P*1 crystal (2PMC). The side chains of only the contacting residues in both the CheY and $CheZ_C$ peptides are shown as ball-and-stick models. The electrostatic contacts are shown as dotted lines, and the hydrophobic interface is illustrated by a dashed green curve.

CheA to CheY in the presence and absence of the $CheZ_{C15}$ peptide were determined. CheY binds to the P2 domain of CheA, and binding of P2 and the $CheZ_C$ peptide to CheY is mutually exclusive since the two binding interfaces on CheY overlap (53). The effect of the $CheZ_C$ peptide on CheA-mediated CheY phosphorylation can be most clearly delineated by using a CheA protein lacking the P2 domain ($CheA_{\Delta P2}$; see Materials and Methods). The in vivo relevance of this deletion construct is discussed below. A similar *E. coli* $CheA_{\Delta P2}$ protein was shown to exhibit 25-fold-slower CheY phosphorylation kinetics than the full-length *E. coli* CheA protein ($CheA_{FL}$), still orders of magnitude faster than CheY phosphotransfer kinetics reported with small-molecule phosphodonors (40).

Since the *E. coli* $CheA_{FL}$ and $CheA_{\Delta P2}$ proteins follow subsecond kinetics of phosphoryl group transfer to CheY, the effect of the presence of the $CheZ_C$ peptide on CheY phosphorylation with the *S. enterica* $CheA_{FL}$ and $CheA_{\Delta P2}$ proteins was investigated using a rapid quench instrument similar to that previously used with the *E. coli* proteins (39, 40). When CheA proteins phosphorylated with [γ-^{32}P]ATP were rapidly mixed with various concentrations of CheY in the presence or absence of the $CheZ_{C15}$ peptide, the intensity of the radiolabeled band corresponding to P∼$CheA_{FL}$ (73 kDa) or P∼$CheA_{\Delta P2}$ (64 kDa) decreased with time due to phosphotransfer while the intensity of the radiolabeled band corresponding to P∼CheY (14 kDa) increased. Due to the greater lability of phospho∼Asp in P∼CheY, the decrease in P∼CheA was used in the kinetic analyses. Observed rate constants (k_{obs}) were obtained by fitting the relative concentration of P∼CheA over time to a single exponential (Fig. 4). First- and second-order phosphorylation rates were estimated from a titration analysis with increasing concentrations of CheY.

Phosphoryl transfer from *S. enterica* P∼$CheA_{FL}$ to CheY followed saturation kinetics (Fig. 5A), as previously observed with *E. coli* proteins (39). Rectangular hyperbola fits to the data (Fig. 5A) defined a first-order rate constant (k_{phos}) of $290 \pm 100\ s^{-1}$ and a K_S value, describing the dissociation of the P∼CheA · CheY complex, of 10.3 ± 2.8 μM, compared to

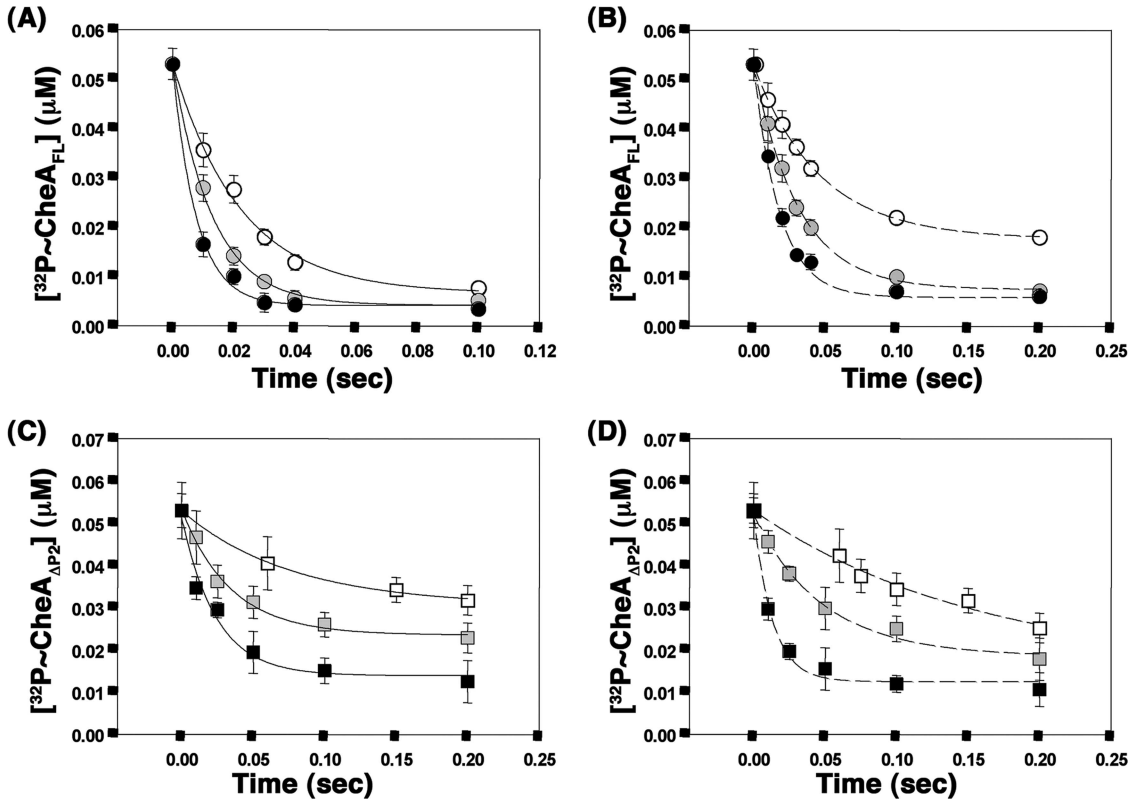

FIG. 4. Single exponential fits to representative data for phosphotransfer from P~CheA to CheY. Phosphoryl transfer from P~CheA$_{FL}$ (A and B) or P~CheA$_{\Delta P2}$ (C and D) to CheY was assayed with 1.4 μM CheY (white), 4.7 μM CheY (gray), or 18.8 μM CheY (black) in the absence (A and C) or presence (B and D) of 2 mM CheZ$_{C15}$ peptide. Single exponential fits used for estimation of k_{obs} are shown. Within each experiment, two aliquots from each time point were analyzed on separate gels, and results were averaged. The data points shown are average values from two independent experiments with the standard errors indicated.

250 ± 40 s^{-1} and 7 ± 2 μM, respectively, previously reported with *E. coli* proteins performed at an identical temperature (8°C) (39). The presence of the CheZ$_{C15}$ peptide in the phosphorylation experiments with P~CheA$_{FL}$ eliminated saturation kinetics, and the calculated second-order rate constant (k_{phos}/K_S) for the CheA$_{FL}$ phosphotransfer reaction (28.2 μM^{-1} s^{-1}) was threefold higher than the observed second-order rate constant in the presence of the CheZ$_{C15}$ peptide (9.3 ± 2.2 μM^{-1} s^{-1}) (Fig. 5A).

Phosphoryl transfer from *S. enterica* P~CheA$_{\Delta P2}$ to CheY also did not follow saturation kinetics (Fig. 5B), similar to that observed for *E. coli* CheA$_{\Delta P2}$ (40). Linear fits of the data defined an effective second-order rate constant (k_{phos}/K_S) of 1.3 ± 0.5 μM^{-1} sec^{-1}, compared to 1.5 μM^{-1} sec^{-1} for *E. coli*

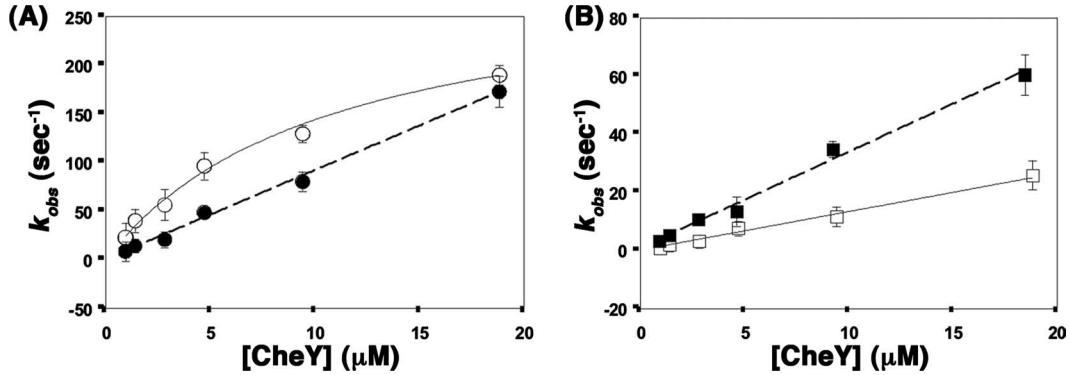

FIG. 5. Kinetic fits to k_{obs} versus [CheY]. Estimates of the k_{obs} value were obtained from phosphotransfer data from P~CheA$_{FL}$ (A) or P~CheA$_{\Delta P2}$ (B) to CheY in the presence (closed symbols) or absence (open symbols) of the CheZ$_{C15}$ peptide. The data corresponding to phosphotransfer from P~CheA$_{FL}$ to CheY in the absence of the CheZ$_{C15}$ peptide are fit to a rectangular hyperbola to define a second-order rate constant, k_{phos}; the remaining data are fit linearly to define first-order rates (k_{phos}/K_S). Error bars denote standard errors of replicates.

$CheA_{\Delta P2}$ at 25°C (40). In the presence of the $CheZ_{C15}$ peptide, phosphoryl transfer from P~$CheA_{\Delta P2}$ still did not follow saturation kinetics but was accelerated by 2.6-fold (Fig. 5B) compared to phosphorylation of peptide-free CheY. Linear fits of the data defined a second-order rate constant, k_{phos}/K_S of $3.4 \pm 1.2\ \mu M^{-1}\ s^{-1}$. The 2.6-fold acceleration of phosphoryl transfer from CheA to CheY in the presence of the $CheZ_{C15}$ peptide contrasts with the 10-fold acceleration of phosphoryl transfer to $CheZ_{C15}$-bound CheY from the small-molecule phosphodonor phosphoramidate (35).

DISCUSSION

Evidence for CheY conformation-specific alternate binding modes of $CheZ_C$. Previous structural studies with $CheZ_{C15}$ peptide-bound complexes of inactive and activated CheY revealed alternate modes of binding of the $CheZ_C$ peptide to CheY that are subject to the conformational state of the CheY protein (Fig. 1). The equilibrium binding studies provide strong biochemical evidence in support of the state-specific dual-binding-mode hypothesis (Table 4). While inactive CheY binds to both the $CheZ_{C19}$ and $CheZ_{C15}$ peptides with similar affinities, the binding affinity of P~CheY is sixfold greater for $CheZ_{C19}$ than for $CheZ_{C15}$. Furthermore, the $CheZ_{C19}$ peptide containing the Gln202Ala and Asp206Ala mutations, which eliminate the active mode-specific contacts, shows close to 10-fold lower affinity for P~CheY and less than 2-fold weaker binding to inactive CheY.

Structural studies of CheY-BeF_3^--$CheZ_{C19}$ revealed additional specific contacts between the switch region in CheY and the extended N terminus in $CheZ_{C19}$, accounting for the lower K_d value for activated CheY binding to $CheZ_{C19}$ than for binding to $CheZ_{C15}$ (Table 4). Further, in the structures of the inactive CheY-$CheZ_{C15}$ complexes, the C terminus of the $CheZ_{C15}$ peptide accounts for a substantial portion of the CheY α4-β5-α5 binding interface while the N terminus is exposed to the solvent (13) (Fig. 3D). With the assumption that $CheZ_{C19}$ binds to inactive CheY using the inactive binding mode, the extended N terminus would be predicted to have little or no effect, accounting for the observed identical binding affinities for inactive CheY with both the $CheZ_{C19}$ and $CheZ_{C15}$ peptides (Table 4).

Molecular recognition by the $CheZ_C$ peptide for inactive and activated CheY. The importance of the CheZ C-terminal Phe214 residue has long been recognized, and several studies have addressed the consequences of mutations at this site. The *cheZ* Phe214Cys mutants in both *E. coli* (5) and *S. enterica* (37) are chemotactic, and a *cheZ* Phe214Leu mutant in *E. coli* displays a gain-of-function phenotype (34). The current study addresses the importance of this residue by explaining the mechanism of molecular recognition in the CheY-$CheZ_C$ interaction. A single-site mutation to Ala ($CheZ_{C19}$ Phe214Ala) drastically impacts binding to both inactive and P~CheY (Table 4). Phe214 is completely buried in the inactive CheY-$CheZ_{C15}$ structures, contributing to >40% of the buried surface at the interface, while it is only partially buried in the activated CheY-$CheZ_C$ structures, contributing to <15% of the buried surface at the interface (13).

The structural and mutational analyses presented in this study establish the role of Phe214 as an anchor residue in the molecular recognition mechanism between $CheZ_C$ and CheY. Phe214 is highly conserved as the C-terminal residue in CheZ proteins of most eubacterial species. A rare exception occurs in *Xanthomonas* spp., where the C-terminal residue is a Leu and residues in CheY that are predicted to form the CheY-$CheZ_C$ interface also differ, consistent with the identification of this residue as a key determinant of molecular recognition. The use of Phe as an anchor is not unique to CheY-$CheZ_C$ recognition in bacterial chemotaxis. The pentapeptide motif (NWETF) present at the C termini of high-copy-number *E. coli* methyl-accepting proteins (Tar and Tsr) also uses the C-terminal Phe to tether methyltransferase CheR for methylation (50).

Evolutionarily conserved anchor residues provide specific side chains that penetrate into a structurally constrained binding groove of the binding partner during molecular recognition between two interacting proteins (32). Such recognition motifs bury the maximum surface area after complexation. The existence of such anchors might allow binding pathways to bypass kinetically expensive structural rearrangements at the binding interface. It is postulated that once the anchors are docked, solvent-exposed flexible side chains latch onto the binding interface at the periphery of the pocket through an induced-fit mechanism.

Consistent with its role as a molecular anchor, Phe214 hooks into the hydrophobic pocket created by the solvent-buried conformation of CheY Tyr106 on its α4-β5-α5 face, irrespective of the phosphorylation or activation state of the active site Asp57, since the rotameric conformation of Tyr106 is almost identical in meta-active CheY of the inactive CheY-$CheZ_{C15}$ structures and in fully activated CheY-BeF_3^- of the $CheZ_{C15}$- and $CheZ_{C19}$-bound structures. However, in the absence of phosphorylation, the lack of complete reorientation of Thr87 and the β4-α4 loop leaves only a hydrophobic patch and the solvent-exposed Lys119 side chain for interaction at the inactive CheY binding interface, rendering the inactive binding mode with the N terminus exposed to the solvent. In contrast, in the presence of phosphorylation, complete reorientation of Thr87 and the β4-α4 loop offers additional contacts for the N terminus of the $CheZ_C$ peptide, which can now latch onto the activated CheY interface using solvent-exposed side chains of Gln202 and Asp206 of $CheZ_C$. In essence, conformation-dependent differences in surface profiles of the α4-β5-α5 signaling face favor binding of the $CheZ_C$ helix in different orientations.

Effect of $CheZ_C$ peptide on CheY phosphorylation kinetics with P~CheA. The $CheZ_C$ peptide-associated acceleration of CheY phosphorylation was previously reported with small-molecule phosphodonors (35). This is the first report investigating the effect of the $CheZ_C$ peptide on CheY phosphorylation with the more physiologically relevant phosphodonor kinase CheA. Phosphoryl transfer from $CheA_{FL}$ to CheY follows saturation kinetics, as previously reported (39), indicating the formation of a P~$CheA_{FL}$ · CheY complex prior to phosphotransfer. The existence of a CheY binding domain on $CheA_{FL}$ (P2) is the basis for the observed saturation. In the presence of the $CheZ_{C15}$ peptide, the rate of phosphorylation is threefold lower and saturation is eliminated, indicating loss of the binding site on CheA for CheY. Binding of $CheZ_C$ and that of CheA-P2 to CheY are mutually exclusive due to steric overlap of the binding sites. With the K_d values reported to be

~2 μM for P2-CheY binding (21) and determined to be ~70 μM for CheZ$_{C15}$-CheY binding, in these experiments, ~97% of the CheY molecules are estimated to exist as a complex with the peptide and CheA-P2 is predicted to compete with the CheZ$_{C15}$ peptide for binding to CheY at the final protein and peptide concentrations used, accounting for the lower rate of phosphoryl transfer. In the absence of the CheA-P2 domain (CheA$_{\Delta P2}$), saturation kinetics is eliminated (40). The presence of the CheZ$_{C15}$ peptide in this case has only a modest effect (2.6-fold) on the rate of phosphoryl transfer to CheY.

It should be noted that one of the CheA$_{FL}$-CheY phosphotransfer time courses in the presence of the CheZ$_{C15}$ peptide (Fig. 4B) and two of the CheA$_{\Delta P2}$-CheY phosphotransfer time courses, in both the absence and presence of the CheZ$_{C15}$ peptide (Fig. 4C and D), reach an equilibrium rather than completion. In all of the above cases, the effective concentration of CheY available to bind to CheA is below the K_d value for CheA-CheY interaction. It is also possible that the rate of reverse phosphotransfer from P~CheY to CheA might be affected by the CheZ$_C$ peptide, although such a conclusion is beyond the scope of this study. In either case, the initial rates of phosphotransfer, and hence conclusions drawn from these observations, are not affected.

Effects of the CheZ$_C$ peptide on phosphotransfer kinetics from P~CheA to CheY are relevant within the context of a bacterial cell. Localization of key components plays an important role in chemotaxis signal transduction. Both the kinase CheA and the phosphatase CheZ localize to the cytoplasmic faces of membrane-bound chemoreceptors that cluster at cell poles (1, 7, 16, 22, 45, 49). This potentially poises CheZ to present CheY to CheA for phosphoryl transfer through the CheZ$_C$-mediated tether. Such a scenario is supported by stoichiometric quantification of chemotaxis components (22), together with estimated binding affinities, imparting an ancillary level of regulation in the form of futile cycles of phosphorylation by CheA and dephosphorylation by CheZ that might play a role in modulating sensitivity in the system (13). Whether the modest 2.6-fold enhancement of CheA-mediated phosphorylation of CheY by CheZ$_C$ binding observed in vitro is itself important or whether it is further amplified in the intracellular environment is still an open question.

ACKNOWLEDGMENTS

We thank the beamline staff at X4A and X4C at the National Synchrotron Light Source at Brookhaven National Laboratory for technical assistance during data collection, Rajiv Bandwar and Guo-Qing Tang for scientific interpretation of the kinetic data, Vasanti S. Anand and Vaishnavi Rajagopal for technical help with the rapid quench instrument, and J. Kavanaugh for the delta rmsd fortran codes.

This work was supported by U.S. National Institutes of Health grant 2R37GM47958. A.M.S. is an investigator of the Howard Hughes Medical Institute.

We have no competing financial interests.

REFERENCES

1. **Ames, P., C. A. Studdert, R. H. Reiser, and J. S. Parkinson.** 2002. Collaborative signaling by mixed chemoreceptor teams in *Escherichia coli*. Proc. Natl. Acad. Sci. USA **99:**7060–7065.
2. **Baker, M. D., P. M. Wolanin, and J. B. Stock.** 2006. Signal transduction in bacterial chemotaxis. Bioessays **28:**9–22.
3. **Baker, M. D., P. M. Wolanin, and J. B. Stock.** 2006. Systems biology of bacterial chemotaxis. Curr. Opin. Microbiol. **9:**187–192.
4. **Blat, Y., and M. Eisenbach.** 1996. Conserved C-terminus of the phosphatase CheZ is a binding domain for the chemotactic response regulator CheY. Biochemistry **35:**5679–5683.
5. **Blat, Y., and M. Eisenbach.** 1996. Oligomerization of the phosphatase CheZ upon interaction with the phosphorylated form of CheY. J. Biol. Chem. **271:**1226–1231.
6. **Brünger, A. T., P. D. Adams, G. M. Clore, W. L. DeLano, P. Gros, R. W. Grosse-Kunstleve, J. S. Jiang, J. Kuszewski, M. Nilges, N. S. Pannu, R. J. Read, L. M. Rice, T. Simonson, and G. L. Warren.** 1998. Crystallography & NMR system: a new software suite for macromolecular structure determination. Acta Crystallogr. D **54:**905–921.
7. **Cantwell, B. J., R. R. Draheim, R. B. Weart, C. Nguyen, R. C. Stewart, and M. D. Manson.** 2003. CheZ phosphatase localizes to chemoreceptor patches via CheA-short. J. Bacteriol. **185:**2354–2361.
8. **Collaborative Computational Project, Number 4.** 1994. The CCP4 suite: programs for protein crystallography. Acta Crystallogr. D **50:**760–763.
9. **Delano, W. L.** 2002. The Pymol molecular graphics system. DeLano Scientific, San Carlos, CA.
10. **Diemand, A. V., and H. Scheib.** 2004. iMolTalk: an interactive, internet-based protein structure analysis server. Nucleic Acids Res. **32:**W512–W516.
11. **French, S., and K. Wilson.** 1978. On the treatment of negative intensity observations. Acta Crystallogr. A **34:**517–525.
12. **Gill, S. C., and P. H. von Hippel.** 1989. Calculation of protein extinction coefficients from amino acid sequence data. Anal. Biochem. **182:**319–326.
13. **Guhaniyogi, J., V. L. Robinson, and A. M. Stock.** 2006. Crystal structures of beryllium fluoride-free and beryllium fluoride-bound CheY in complex with the conserved C-terminal peptide of CheZ reveal dual binding modes specific to CheY conformation. J. Mol. Biol. **359:**624–645.
14. **Kantardjieff, K. A., and B. Rupp.** 2003. Matthews coefficient probabilities: improved estimates for unit cell contents of proteins, DNA, and protein-nucleic acid complex crystals. Protein Sci. **12:**1865–1871.
15. **Kavanaugh, J. S., J. A. Weydert, P. H. Rogers, and A. Arnone.** 1998. High-resolution crystal structures of human hemoglobin with mutations at tryptophan 37β: structural basis for a high-affinity T-state. Biochemistry **37:**4358–4373.
16. **Kim, K. K., H. Yokota, and S.-H. Kim.** 1999. Four-helical-bundle structure of the cytoplasmic domain of a serine chemotaxis receptor. Nature **400:**787–792.
17. **Kleywegt, G. J., and T. A. Jones.** 1998. Databases in protein crystallography. Acta Crystallogr. D **54:**1119–1131.
18. **Lamzin, V. S., and K. S. Wilson.** 1993. Automated refinement of protein models. Acta Crystallogr. D. **49:**129–147.
19. **Lee, S. Y., H. S. Cho, J. G. Pelton, D. Yan, E. A. Berry, and D. E. Wemmer.** 2001. Crystal structure of activated CheY. J. Biol. Chem. **276:**16425–16431.
20. **Levin, M. K., and S. S. Patel.** 2002. Helicase from hepatitis C virus, energetics of DNA binding. J. Biol. Chem. **277:**29377–29385.
21. **Li, J., R. V. Swanson, M. I. Simon, and R. M. Weis.** 1995. The response regulators CheB and CheY exhibit competitive binding to the kinase CheA. Biochemistry **34:**14626–14636.
22. **Li, M., and G. L. Hazelbauer.** 2004. Cellular stoichiometry of the components of the chemotaxis signaling complex. J. Bacteriol. **186:**3687–3694.
23. **Lukat, G. S., W. R. McCleary, A. M. Stock, and J. B. Stock.** 1992. Phosphorylation of bacterial response regulator proteins by low molecular weight phospho-donors. Proc. Natl. Acad. Sci. USA **89:**718–722.
24. **Matthews, B. W.** 1968. Solvent content of protein crystals. J. Mol. Biol. **33:**491–497.
25. **Mayover, T. L., C. J. Halkides, and R. C. Stewart.** 1999. Kinetic characterization of CheY phosphorylation reactions: comparison of P-CheA and small-molecule phosphodonors. Biochemistry **38:**2259–2271.
26. **McEvoy, M. M., A. Bren, M. Eisenbach, and F. W. Dahlquist.** 1999. Identification of the binding interfaces on CheY for two of its targets, the phosphatase CheZ and the flagellar switch protein FliM. J. Mol. Biol. **289:**1423–1433.
27. **Messing, J.** 1983. New M13 vectors for cloning. Methods Enzymol. **101:**20–78.
28. **Murshudov, G. N., A. A. Vagin, and E. J. Dodson.** 1997. Refinement of macromolecular structures by the maximum-likelihood method. Acta Crystallogr. D **53:**240–255.
29. **Otwinowski, Z., and W. Minor.** 1997. Processing of X-ray diffraction data collected in oscillation mode. Methods Enzymol. **276:**307–326.
30. **Painter, J., and E. A. Merritt.** 2005. A molecular viewer for the analysis of TLS rigid-body motion in macromolecules. Acta Crystallogr. D **61:**465–471.
31. **Painter, J., and E. A. Merritt.** 2006. Optimal description of a protein structure in terms of multiple groups undergoing TLS motion. Acta Crystallogr. D **62:**439–450.
32. **Rajamani, D., S. Thiel, S. Vajda, and C. J. Camacho.** 2004. Anchor residues in protein-protein interactions. Proc. Natl. Acad. Sci. USA **101:**11287–11292.
33. **Rossmann, M. G.** 1990. The molecular replacement method. Acta Crystallogr. A **46:**73–82.
34. **Sanna, M. G., and M. I. Simon.** 1996. In vivo and in vitro characterization of *Escherichia coli* protein CheZ gain- and loss-of-function mutants. J. Bacteriol. **178:**6275–6280.
35. **Schuster, M., R. E. Silversmith, and R. B. Bourret.** 2001. Conformational coupling in the chemotaxis response regulator CheY. Proc. Natl. Acad. Sci. USA **98:**6003–6008.

36. **Sheridan, R. C., J. F. McCullough, and Z. T. Wakefield.** 1971. Phosphoramidic acid and its salts. Inorg. Synth. **13:**23–26.
37. **Silversmith, R. E.** 2005. High mobility of carboxyl-terminal region of bacterial chemotaxis phosphatase CheZ is diminished upon binding divalent cation or CheY-P substrate. Biochemistry **44:**7768–7776.
38. **Simms, S. A., A. M. Stock, and J. B. Stock.** 1987. Purification and characterization of the *S*-adenosylmethionine: glutamyl methyltransferase that modifies membrane chemoreceptor proteins in bacteria. J. Biol. Chem. **262:** 8537–8543.
39. **Stewart, R. C.** 1997. Kinetic characterization of phosphotransfer between CheA and CheY in the bacterial chemotaxis signal transduction pathway. Biochemistry **36:**2030–2040.
40. **Stewart, R. C., K. Jahreis, and J. S. Parkinson.** 2000. Rapid phosphotransfer to CheY from a CheA protein lacking the CheY-binding domain. Biochemistry **39:**13157–13165.
41. **Stock, A., T. Chen, D. Welsh, and J. Stock.** 1988. CheA protein, a central regulator of bacterial chemotaxis, belongs to a family of proteins that control gene expression in response to changing environmental conditions. Proc. Natl. Acad. Sci. USA **85:**1403–1407.
42. **Stock, A., D. E. Koshland, Jr., and J. Stock.** 1985. Homologies between the *Salmonella typhimurium* CheY protein and proteins involved in the regulation of chemotaxis, membrane protein synthesis, and sporulation. Proc. Natl. Acad. Sci. USA **82:**7989–7993.
43. **Stock, A. M., J. M. Mottonen, J. B. Stock, and C. E. Schutt.** 1989. Three-dimensional structure of CheY, the response regulator of bacterial chemotaxis. Nature **337:**745–749.
44. **Storoni, L. C., A. J. McCoy, and R. J. Read.** 2004. Likelihood-enhanced fast rotation functions. Acta Crystallogr. D **60:**432–438.
45. **Studdert, C. A., and J. S. Parkinson.** 2004. Crosslinking snapshots of bacterial chemoreceptor squads. Proc. Natl. Acad. Sci. USA **101:**2117–2122.
46. **Tabor, S., and C. C. Richardson.** 1985. A bacteriophage T7 RNA polymerase/promoter system for controlled exclusive expression of specific genes. Proc. Natl. Acad. Sci. USA **84:**1074–1078.
47. **Vriend, G.** 1990. WHAT IF: a molecular modeling and drug design program. J. Mol. Graph. **8:**52–56, 29.
48. **Wadhams, G. H., and J. P. Armitage.** 2004. Making sense of it all: bacterial chemotaxis. Nat. Rev. Mol. Cell Biol. **5:**1024–1037.
49. **Wang, H., and P. Matsumura.** 1996. Characterization of the $CheA_s$/CheZ complex: a specific interaction resulting in enhanced dephosphorylating activity on CheY-phosphate. Mol. Microbiol. **19:**695–703.
50. **Wu, J., J. Li, G. Li, D. G. Long, and R. M. Weis.** 1996. The receptor binding site for the methyltransferase of bacterial chemotaxis is distinct from the sites of methylation. Biochemistry **35:**4984–4993.
51. **Yan, D., H. S. Cho, C. A. Hastings, M. M. Igo, S. Y. Lee, J. G. Pelton, V. Stewart, D. E. Wemmer, and S. Kustu.** 1999. Beryllofluoride mimics phosphorylation of NtrC and other bacterial response regulators. Proc. Natl. Acad. Sci. USA **96:**14789–14794.
52. **Zhao, R., E. J. Collins, R. B. Bourret, and R. E. Silversmith.** 2002. Structure and catalytic mechanism of the *E. coli* chemotaxis phosphatase CheZ. Nat. Struct. Biol. **9:**570–575.
53. **Zhu, X., K. Volz, and P. Matsumura.** 1997. The CheZ-binding surface of CheY overlaps the CheA- and FliM-binding surfaces. J. Biol. Chem. **272:** 23758–23764.